ADVANCED FUNCTIONAL MATERIALS
www.afm-journal.de



# Nanostructured Polymer Brushes by UV-Assisted Imprint Lithography and Surface-Initiated Polymerization for Biological Functions

*Edmondo M. Benetti, Canet Acikgoz, Xiaofeng Sui, Boris Vratzov, Mark A. Hempenius, Jurriaan Huskens,* and G. Julius Vancso**

Dedicated to Prof. Marcus Textor on the occasion of his 65th birthday

**Functional polymer brush nanostructures are obtained by combining step-and-flash imprint lithography (SFIL) with controlled, surface-initiated polymerization (CSIP). Patterning is achieved at length scales such that the smallest elements have dimensions in the sub-100 nm range. The patterns exhibit different shapes, including lines and pillars, over large surface areas. The platforms obtained are used to selectively immobilize functional biomacromolecules. Acrylate-based polymer resist films patterned by SFIL are first used for the selective immobilization of ATRP silane-based initiators, which are coupled to unprotected domains of silicon substrates. These selectively deposited initiators are then utilized in the controlled radical SIP of poly(ethylene glycol)methacrylates (PEGMA). Nanostructured brush surfaces are then obtained by removal of the resist material. The areas previously protected by the SFIL resist are passivated by inert, PEG-based silane monolayers following resist removal. PEGMA brush nanostructures are finally functionalized with biotin units in order to provide selective attachment points for streptavidin proteins. Atomic force microscopy and fluorescence spectroscopy confirm the successful immobilization of streptavidin molecules on the polymer grafts. Finally, it is demontrated that this fabrication method allows the immobilization of a few tens of protein chains attached selectively to brush nanostructures, which are surrounded by nonfouling PEG-functionalized areas.**

## 1. Introduction

Functional polymer brushes have been used with increasing success for tailoring the chemical and physical characteristics of a large variety of surfaces, including metallic and non-metallic susbtrates.[1–3] Their success is, among others, related to a swift development in controlled surface-initiated polymerization (CSIP) approaches[4] which allow one to obtain chemically and topologically patterned brush layers with well-defined properties, such as, thickness and functionalities.

The coupling of lithographic techniques for the confined modification of surfaces on the nano-scale on the one hand, and CSIP methods on the other hand, has provided additional control over the composition, shape, and dimensions of the features in nanostructured polymer brushes.[5–9] Full control of these parameters is needed, for instance, for the preparation of macromolecular sensors, platforms for single-protein studies, and novel nanofluidic devices. Among these applications the ability to pattern biomolecules to surfaces

Prof. G. J. Vancso
Materials Science and Technology of Polymers
MESA+ Institute for Nanotechnology
University of Twente
P.O. Box 217, 7500 AE Enschede, The Netherlands
E-mail: g.j.vancso@utwente.nl
Dr. C. Acikgoz,[†] X. Sui, Dr. M. A. Hempenius
Materials Science and Technology of Polymers
MESA+ Institute for Nanotechnology
University of Twente
P.O. Box 217, 7500 AE Enschede, The Netherlands
Prof. J. Huskens
Molecular Nanofabrication Group
MESA+ Institute for Nanotechnology
University of Twente
P.O. Box 217, 7500 AE Enschede, The Netherlands
E-mail: j.huskens@utwente.nl
Dr. E. M. Benetti,[†]
ETH Zürich, Dept. of Materials
Laboratory for Surface Science and Technology
Wolfgang Pauli Strasse 10, HCI G543, 8093 Zürich, Switzerland
Dr. B. Vratzov
NT&D–Nanotechnology and Devices
Wirichsbongardstr. 24, 52062 Aachen, Germany
[†] These authors contributed equally to this work.

DOI: 10.1002/adfm.201002569

is of great importance in, for example, biotechnology, biosensors,[10] immune assays,[11] and cell-adhesion studies. Current methods of protein patterning include both "top-down" techniques such as microcontact printing,[12,13] or e-beam lithography[14,15] and "bottom-up" methods such as block copolymer and particle lithography.[16–19] All these approaches rely on the combination of micro/nanofabrication for localized surface modification and the subsequent chemical activation aimed at specific protein immobilization. So far the combination of self-assembled monolayers (SAMs) (e.g., patterned by soft lithography) and polymer brushes[20] have been successfully applied as chemically tunable platforms to obtain patterns of active sites that recognize and bind proteins.

Structuring of surfaces on the nanoscale using CSIP-based lithographies has enabled the preparation of brush nanostructures on flat surfaces (named as nanobrushes[21] or brush "hedges"[22,23]). This process is generally based on the localized delivery of precursors for polymerization (i.e., initiator adsorbates or molecular species, which can be later activated to become initiators) followed by the laterally confined grafting of a polymer. The pattern resolution and feature shapes are determined by the fabrication of the SAMs. Inertness of the unpatterned domains is a very important requirement as the CSIP process must be selectively carried out on the activated positions and undesired secondary effects by the surrounding substrate (either physisorption of the polymer from solution during CSIP or polymerization initiated by defects on the surface) must be avoided.

Suitable methods to modify the nanoscale precursor surfaces for subsequent CSIP have been mainly based on electron-beam lithography (EBL),[9,24,25] atomic force microscopy (AFM) lithography,[6–8] and soft-lithography techniques.[26,27] These approaches have been frequently used in combination with CSIP following single or multiple fabrication steps. In this way functional brush nanostructures with typical lateral resolutions down to a few tens of nanometers have been obtained.[22,23] However, these CSIP-based lithographies are affected by several limiting factors. Brush patterning by EBL- and AFM-based approaches imply high costs and they do not allow the preparation of "large" patterned areas. Alternatively, soft lithographic methods, despite their high reproducibility and low cost, are limited to relatively low lateral resolutions.

The above-mentioned drawbacks could be overcome by applying high-throughput processes, such as nanoimprint lithography (NIL),[28,29] for surface modification in combination with CSIP. Nanoimprint lithography has shown great promise as it is a low-cost process that allows the patterning of large areas and simultaneously achieves high pattern resolutions.[28,29] In thermal NIL, mold patterns are replicated into a thermoplastic material by heating the polymer above its glass transition temperature and applying a pressure on the mold.[28]

Step-and-flash imprint lithography (SFIL),[30–32] a UV-NIL variant, is particularly attractive because of the high feature density that can be obtained and the high efficiency in replicating multiple and complex pattern types on the same mold.[30] In SFIL, a low viscosity, photocurable liquid or solution is dispensed in the form of small droplets (as opposed to spin coating) onto the substrate to fill the voids of a quartz mold. Exposing this solution to UV light cures the photopolymer to make a solidified replica while in contact with the mold. Removing the mold leaves the inverse replica on the substrate. This method does not require temperature cycling, as in the thermal NIL process, leading to a higher throughput, and the transparency of the template offers the possibility for easy optical and high-precision alignment. Because of the ability to pattern at room temperature and at low pressure, the template can be used to pattern the whole wafer area as in a stepper-lithography tool. These advantages thus enable the fabrication of different types of patterns on the same substrate, reproduced over large areas, and with lateral sizes ranging from several micrometers down to the sub-50 nm range (see **Figure 1**).[33]

We explore here the combination of SFIL with CSIP, which allows one to couple the initiators for polymerization that are delivered selectively to unprotected areas of substrates featuring resist patterns. This strategy enables the selective functionalization of large precursor surfaces with high specificity and negligible contamination on the areas protected by the imprinted resist. Subsequent CSIP allows the fabrication of a variety of nanopatterned brush structures presenting a wide range of pattern sizes as determined by the resist structure, down to

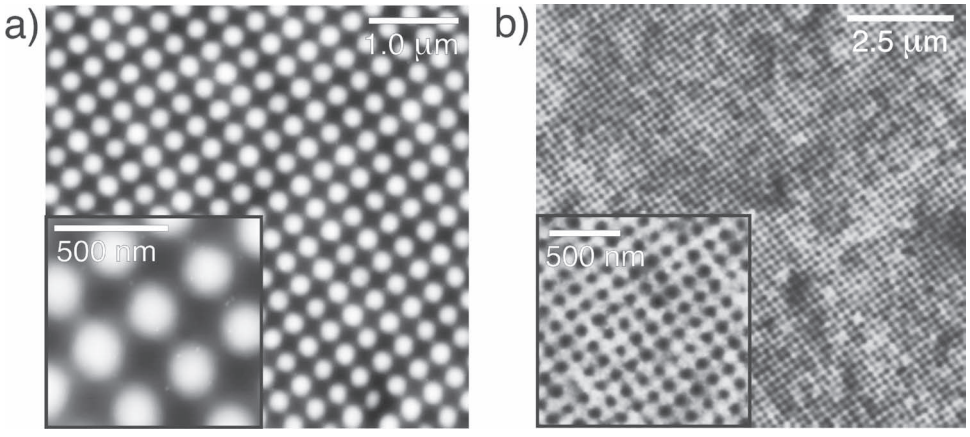


**Figure 1.** Representative AFM tapping-mode height images depicting PEGMA nanopatterned brushes fabricated by the SFIL/SI-ATRP process; a) 200-nm wide pillars and b) 70-nm hollow structures. PEGMA brushes were successfully patterned on large areas and presented uniform and regular structures (height scale from black to white 100 nm).

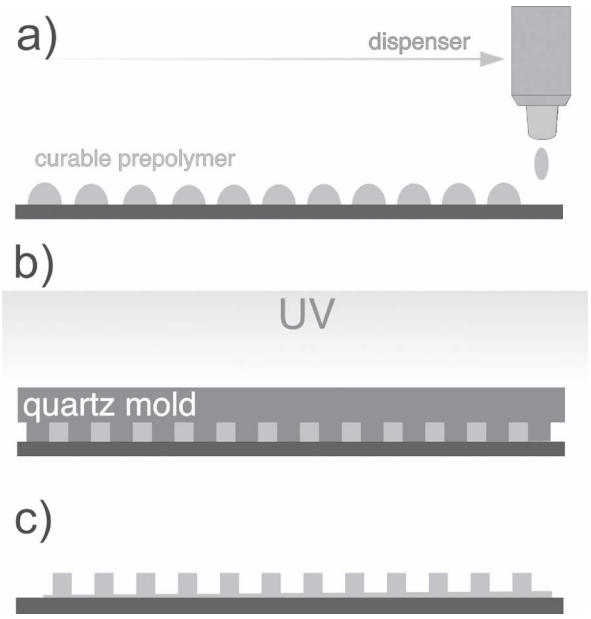


**Scheme 1.** Schematic depiction of the step-and-flash nanoimprint process: a) uniform dispensing of curable resist solution, b) application of the quartz mold and curing by UV light, and c) demolding.

a few tens of nanometers and with high reproducibility over large areas. Motivated by the high performances and versatility shown by SFIL, we report on a new approach for the preparation of diverse polymer-brush nanopatterns directly grafted on silicon oxide surfaces and with typical dimensions ranging from several micrometers down to sub-100 nanometers using the above described combination of SFIL and CSIP.

The fabrication method used (summarized in **Scheme 1**) is based on the SFIL patterning of a polyacrylate-based resist film,[34,35] followed by etching of inter-feature residual layers, which assured the selective exposure of unpatterned $SiO_x$ surface domains. As for the CSIP we chose atom-transfer radical polymerization (ATRP). Silane-based initiators for surface-initiated ATRP (SI-ATRP)[36] were delivered by vapor deposition onto the exposed areas of $SiO_x$ substrates. Confined grafting of [poly(ethylene glycol)]polymethacrylate (PEGMA) chains was subsequently performed. Following lift-off of the resist patterns, well-defined brush nanostructures regularly spaced by bare $SiO_x$ were obtained.

In order to test the application of the so-fabricated brush platforms for specific protein immobilization, areas exposing the underlying substrate were initially passivated with silane-terminated oligo(ethylene glycol) (Si-OEG) SAMs. Thus, non-specific protein adsorption in the unprotected areas of the nanostructures was prevented. The PEGMA brushes were subsequently modified with succinic anhydride (SA)[23] and activated by 1-ethyl-3-(3-dimethylaminopropyl)-carbodiimide (EDC)/*N*-hydroxysuccinimide (NHS) for subsequent amino-biotin functionalization. Decoration of the brush chains with biotin functions further allowed the selective adsorption of streptavidin proteins.

The chemical composition of the prepared platforms, following every functionalization step, was investigated by Fourier-transform infrared (FTIR) spectroscopy. The morphology and size of the PEGMA brush nanostructures were step-by-step monitored by high-resolution AFM demonstrating how brush lines and pillars with typical widths ranging from hundreds to a few tens of nanometers could be fabricated. Fluorescence spectroscopy further demonstrated the successful immobilization of dyed streptavidin selectively on the patterned areas, whereas analysis of the AFM images confirmed the formation of protein patterns consisting of a few tens of biomolecules.

## 2. Results and Discussion

First we provide an overview of the patterning process used (**Scheme 2**) depicting the steps of the fabrication of PEGMA brush nanostructures via the combination of SFIL[30] and SI-ATRP, and the subsequent preparation of brush-protein conjugates. In the SFIL process the acrylate-based resist material was dispensed onto the transfer-layer coated substrates and an appropriate template was subsequently brought into contact with the liquid resist (Scheme 2a). The transfer layer provided good adhesion of the resist material to the substrate. Following UV exposure and curing of the resist the template was demolded from the substrate obtaining its negative 3D image (Scheme 2b). In order to expose the underlying silicon substrate in the grooves of the imprinted structures, the residual layer was removed by oxygen plasma (Scheme 2c).

The patterned resist substrates were then reacted with the ATRP initiator (see Experimental Section for details on the synthesis) thus forming initiating SAMs on the exposed unprotected domains spaced by resist patterns (Scheme 2d). PEGMA brushes were then grown from the ATRP initiator-SAMs affording brush nanostructures of different shapes and sizes (Scheme 2e). Following SI-ATRP, the resist lines were removed by sonication after which brush nanostructures spaced by areas exposing the bare silicon substrate were obtained (Scheme 2f).

The mold used in the SFIL process featured patterns consisting of 500-nm to 100-nm wide lines with pitches of 1:1, 1:2, 1:3, 1:4, 1:5 and with a valley-to-mesa height of 100 nm (see Supporting Information (SI), Figure S1). In addition, the template included pillars and grooves with widths between 70 and 200 nm.

From the cross-sectional scanning electron microscopy (SEM) images of the imprinted lines (SI, Figure S1) it can be seen that the combined thickness of the transfer layer and the residual UV-cured resist following imprinting was about 40 nm. As earlier mentioned, in order to remove this residual layer, the imprinted samples were subsequently treated with oxygen plasma. As a result, 150-nm high resist patterns were obtained, featuring areas where the bare $SiO_x$ was exposed[29] (SI, Figure S1). Following the etching step the unprotected regions were selectively functionalized with the ATRP initiator to allow the subsequent grafting of PEGMA brushes.

Preparation of PEGMA brushes by SI-ATRP was earlier reported by Klok et al.[37] and Chikoti et al.[38] In our case the synthesis of PEGMA brushes was accomplished by ATRP[39,40] in aqueous media, using $CuCl/CuBr_2$/bipyridine[41] as a catalyst system (see Experimental Section for details). By this

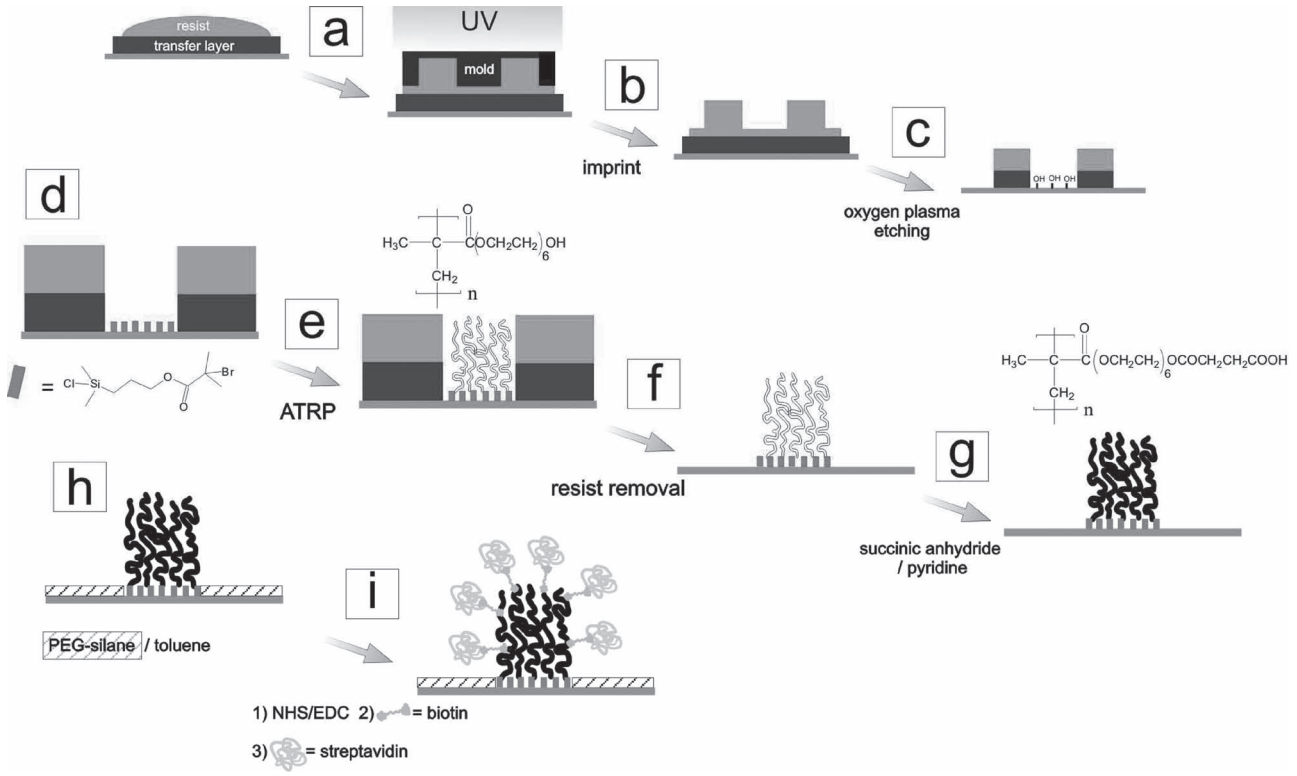


**Scheme 2.** Step-wise fabrication process for creating protein-immobilized PEGMA brush nanostructures.

polymerization procedure thick brush films were obtained in just 1 hour of reaction time and the absence of organic solvents assured the stability of the resist lines used as a template for brush structuring. The average film thickness was measured by ellipsometry on unpatterned areas exhibiting uniform brush films with a thickness value of approximately 75 nm.

After removal of the resist patterns by short sonication in acetone, PEGMA brush nanostructures of different shapes and lateral sizes were obtained over large areas on the substrates and with high reproducibility for several tests performed (Figure 1). In order to confirm the effective dissolution of the imprinted resist and subsequent exposure of the bare $SiO_x$ surface, tapping-mode (TM) AFM phase analysis and high-resolution SEM were performed on the samples studied. The surface of bare substrates was observed from the SEM images and the absence of any residual resist materials was confirmed by the AFM phase analysis, which showed a sharp alternate contrast between the brush features and the bare $SiO_x$ (SI, Figure S2). In order to demonstrate the presence of bare $SiO_x$ and, thus, the quantitative removal of the resist film, FTIR analysis was also performed on continuous resist films before and after oxygen plasma etching. From this test no detectable traces of resist material were found (data not shown).

In order to investigate the lateral resolution and the morphology of the PEGMA brush nanostructures a series of lines with average line-width ranging from 520 ± 7 to 8 ± 10 nm (**Figure 2**a–e) and brush pillars exhibiting average diameters of 130, 140, and 200 nm (Figure 2f–h) were analyzed by tapping-mode AFM.

The average width of the brush lines was specified using the inter-feature spacing between the resist patterns used as templates in SFIL, as provided by the template pattern.[42,43] In **Figure 3**a the average brush line-width is plotted as a function of the starting initiator-pattern size. As it can be seen, for all brush nanostructures obtained, the average brush width exceeded the corresponding initiator-pattern size by 20–50%.

In several recent studies nano-patterned polymer brushes prepared by "grafting-from" approaches presented increasing widening with decreasing dimensions of the initiator-patterned areas. This effect was attributed to the release of osmotic pressure inside the brush structure that induced a lateral extension of the chains beyond the grafting region.[22,42,44] For brush lines with lateral sizes that are comparable to their height (few tens of nanometers) this effect was found to be more enhanced. It is interesting to note that also in the present study, the prepared brush lines did show a certain widening compared to the starting initiator patterns. However, the relative increase of the width did not depend on the brush line thickness but it was rather constant in all cases studied.

The height of the PEGMA brush lines as a function of the nominal pattern size is captured in Figure 3b. For "nominal" pattern size values of approximately 100 nm, the brush thickness reaches a value that exceeds the average thickness of a uniform PEGMA brush (75 nm); for pattern lines with widths above 100 nm, the brush thickness is even higher. The height of the PEGMA brush lines was found to be comparable to the average thickness of a uniform PEGMA brush film (around 75 nm) only in the cases of brush lines with widths above

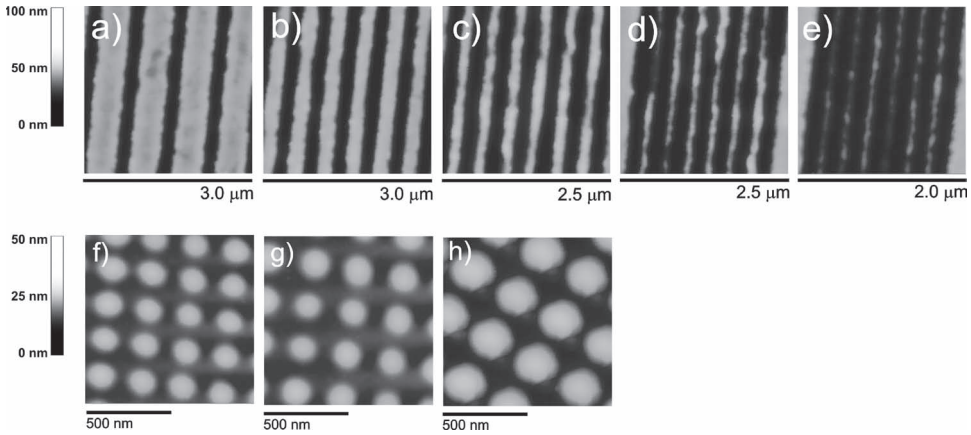


**Figure 2.** Tapping-mode AFM images displaying PEGMA brush nanostructures fabricated by SFIL/SI-ATRP. A series of brush lines (a–e) characterized by line-width values ranging from 520 ± 7 to 80 ± 10 nm and pillars presenting average diameters of 130, 140, and 200 nm (f–h) are shown.

100 nm. For sub-100 nm lines the average brush height was much lower, namely, only about 30 nm for an 80-nm pattern width. This reduced height was ascribed to the limited diffusion of PEGMA macromonomers during SI-ATRP when the neighboring resist patterns are spaced by just a few tens of nanometers.

The brush nanostructures obtained were subsequently chemically modified in order to function as selective adsorption sites for protein immobilization. Nano-patterned platforms must fulfill specific requirements in order to be used in biological applications, the most important is to create bio-interactive sites in a non-interactive (passivated) background.[17] In order to achieve this, here we chemically coupled a biotin/streptavidin protein system onto PEGMA brushes[37,45] which were previously shown to prevent unspecific protein adsorption.[46] The hydroxyl termini of the PEG segments were functionalized with biotin molecules via SA/NHS. Subsequently, streptavidin units adsorbed on the brush surface by biotin-mediated specific interactions.[23] The anti-fouling character of the PEGMA brush assured a high ratio of specific to non-specific protein binding.[47] Furthermore, in order to achieve a selective immobilization onto the brush nanostructures avoiding non-specific adsorption to the surrounding substrate, exposed silicon oxide regions were passivated by functionalization with PEG-silane species (Scheme 2g–i; see Experimental Section and SI, Figure S3 for details).

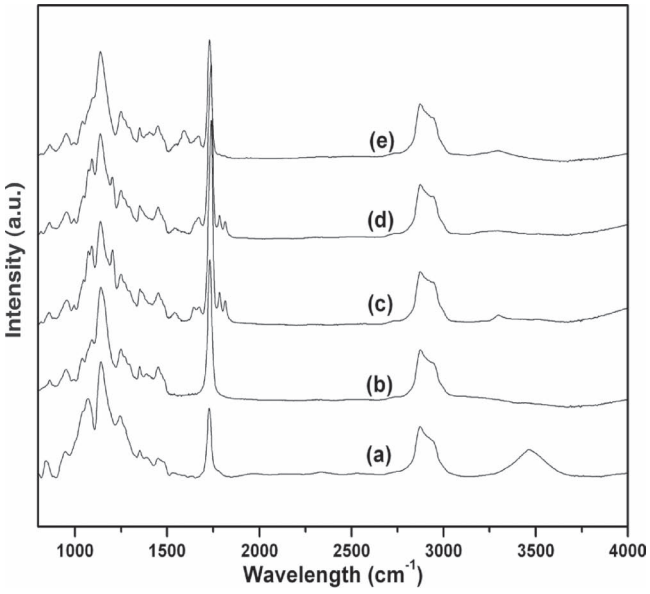


**Figure 4.** FTIR spectra obtained for a) PEGMA brushes, b) PEGMA reacted with SA, c) after reaction with NHS-EDC, d) following amide bond formation with biotin, and e) final reaction with streptavidin.

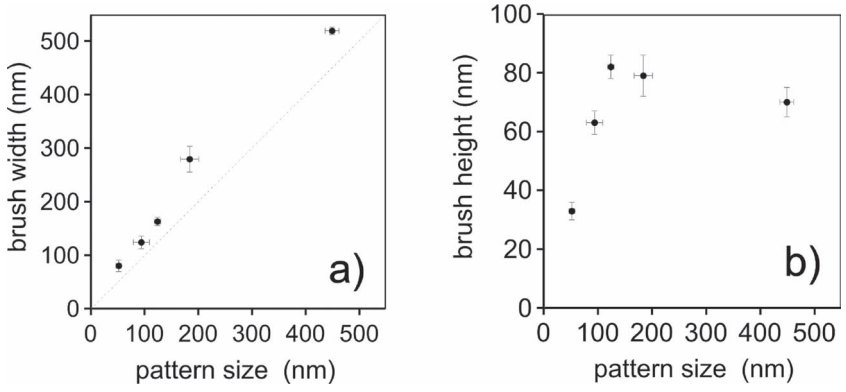


**Figure 3.** Graphs showing a) the width of brush patterns b) the height profile plotted as a function of the starting initiator-pattern size.

In order to assess each functionalization step, FTIR spectra were recorded on uniformly grafted brush films (**Figure 4**), whereas fluorescence microscopy (**Figure 5**) and AFM (**Figure 6**) were used to investigate the changes occurring on the brush nanostructures after modification. Uniform PEGMA brush samples were incubated for 10 h in a dry pyridine solution of SA to introduce carboxylic acid functionalities into the polymer backbones. Following the reaction, the average brush thickness increased

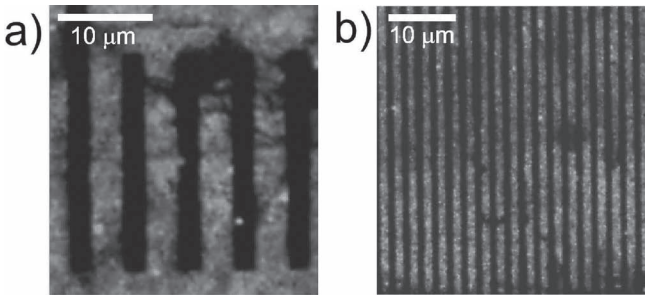


**Figure 5.** Fluorescence microscopy images of PEGMA brush micropatterns functionalized with biotin/dye-labeled streptavidin.

by 20% (as measured by ellipsometry) because of the expected volume increase of the monomer units (Scheme 2g).

The FTIR spectrum of the PEGMA films featured two major absorption bands at 1700 and 1140 $cm^{-1}$ arising from the stretching of the ester carbonyl group and the C-O-C group, respectively (Figure 4a). In addition, a broad band centered at 3500 $cm^{-1}$ originated from the stretching of OH groups in the side PEG segments. As it can be seen in Figure 4b, following functionalization with SA, the relative intensity of the peak at 1700 $cm^{-1}$ markedly increased and the OH-related band disappeared confirming the reaction of the hydroxyl groups and the introduction of carboxylic acid functions along the brush structure.[48]

Carboxylic acid moieties on the PEG segments subsequently reacted with NHS in the presence of EDC thus forming NHS-ester functions that are susceptible to nucleophilic attack and replacement by amino-biotin molecules.[49,50] After the PEGMA brush films had reacted with NHS-EDC the FTIR adsorption spectra was characterized by two signals at 1710 $cm^{-1}$ and 1720 $cm^{-1}$ assigned to the carbon stretching of NHS-ester groups, whereas a signal corresponding to C-N stretching appeared at 1070 $cm^{-1}$ (Figure 4c). Reaction with biotin-PEG(10)-$NH_2$ resulted in a peak at 1680 $cm^{-1}$ because of amide formation following the coupling to carboxylic acid moieties of the PEGMA brush (Figure 4d).

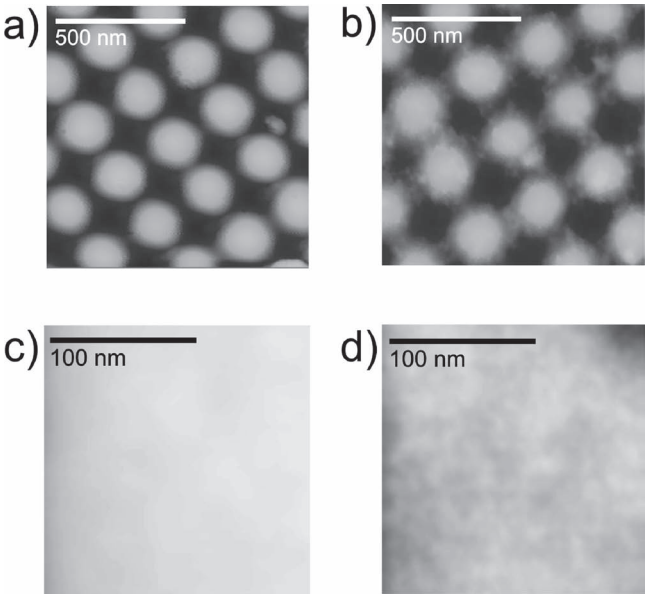


**Figure 6.** TM-AFM images of biotin-PEGMA brush pillars before (a,c) and after immobilization of streptavidin proteins (b,d).

Following each functionalization step PEGMA brush pillars with an initial average diameter of 130 nm (Figure 2f) were analyzed by TM-AFM in the dry state in order to evaluate the average volume increase (Figure S5, SI). We found that the initial average volume occupied by the PEGMA brush pillars measured following SI-ATRP increased by 35% after the attachment of biotin-PEG(10)-$NH_2$. Biotin-modified PEGMA brushes were subsequently incubated in the presence of dye-labeled streptavidin and analyzed by FTIR, TM-AFM, and fluorescence microscopy.

The FTIR spectra recorded on flat brush films confirmed the successful adsorption of streptavidin units as indicated by the appearance of absorption bands corresponding to amide I and II vibrations at 1700–1600 $cm^{-1}$ and 1600–1500 $cm^{-1}$, respectively (Figure 4e). Further evidence for the formation of biotin-streptavidin conjugates was provided by fluorescence microscopy (Figure 5) performed on micro-patterned PEGMA brush structures prepared by the same SFIL/SI-ATRP modification protocol but employing microstructured templates. As it can be seen in Figure 4a and b for 3.5 and 1-μm wide brush patterns, the green areas indicate the presence of dye-labeled streptavidin (see Experimental Section for details), coinciding with the brush surface. This result provides additional support that streptavidin binding occurs only on the biotinated-brush structures and not on regions previously passivated by PEG-silane SAMs.

Comparison of TM-AFM images before (Figure 6a) and after (Figure 6b) incubation in streptavidin solution confirmed the selective adsorption of proteins to the brush nanostructures. As it can be seen in Figure 6b and in the high-resolution image in Figure 6d, protein aggregates decorated the brush surfaces whereas no deposition was recorded in the areas surrounding the PEGMA nanostructures. An estimate of the number of streptavidin units adsorbed on each pillar could be performed by measuring the average volume increase following streptadivin immobilization (see Experimental Section for details).[51] Volume changes were measured over a series of 30 pillars in different positions on the same patterned areas and an average increase by 2% for streptavidin-brush conjugates was found. Considering the theoretical size of one streptavidin unit as 5 nm × 5 nm × 5 nm, we estimated that between 50 and 100 proteins could be adsorbed on each PEG-PMA brush pillar.

## 3. Conclusion

We reported here on the combination of SFIL/SI-ATRP for the preparation of functional brush nanostructures with typical dimensions ranging from several hundreds to a few tens of nanometers. The outlined method allowed the fabrication of different types of nanoscale patterns, e.g., lines or pillars on large substrate areas.

Resist patterns spaced by bare $SiO_x$ were first fabricated by SFIL and these imprinted films subsequently acted as platforms for the selective immobilization of ATRP silane-based initiators. Subsequent grafting of PEGMA brushes in the unprotected areas was achieved by ATRP in aqueous media. Nanostructured

brush surfaces were finally obtained via removal of the resist material. Using this sequential fabrication approach the average size of the brush nanostructures was precisely determined by the morphology of the imprinted resist.

PEGMA brush nanostructures were subsequently chemically coupled to biotin molecules in order to function as selective anchoring points for the subsequent adsorption of streptavidin. The immobilization of a few tens of protein units, selectively attached through biotin ligands onto PEGMA nanostructures and surrounded by non-fouling PEG-functionalized areas was finally accomplished. As it was demonstrated here the combination of SFIL/SI-ATRP and "easy" post-functionalization procedures allowed the fabrication of nanostructured brush platforms that may be successfully applied for specific protein recognition and immobilization. Alternatively, as has been reported before, similar brush-supported protein patterns could be integrated in microfluidic devices[52] for the designing of sensors and bio-reactors paving the way for novel approaches in lab-on-a-chip technologies.

## 4. Experimental Section

*Step-and-Flash Imprint Process*: resist patterns were generated using UV-based nanoimprint technology. All the imprints were carried out on an Imprio 55 (Molecular Imprints Inc.), using their SFIL process. As a substrate, double-sided polished Si wafers were used, which were also coated with a thin transfer layer applied by spin coating and hot baking in order to achieve a good adhesion of the imprint material to the substrate. DUV 30J was used as the transfer layer. The quartz template employed for the imprints consisted of lines with feature sizes from tens of micrometers down to sub-50-nm. Prior to imprinting, the template was treated with a release layer in order to prevent sticking of the imprint material to the template. The release layer was perfluoro-1,1,2,2-tetrahydrooctyltrichlorosilane, which was used to modify the template surface energy. The surface-treatment procedure used in this process started with the cleaning of the template with a piranha solution (conc. $H_2SO_4$ and 33% aq. $H_2O_2$ in a 3:1 volume ratio, *Warning! piranha should be handled with caution; it can detonate unexpectedly*) for 30 min to remove any surface organic contaminants. After the piranha treatment, the substrates were blown dry with $N_2$ and reacted with alkyltrichlorosilane (Aldrich). Imprinting was performed using a low-viscosity acrylate-based organic SFIL resist (Monomat, Molecular Imprints Inc.). The imprint material was deposited by direct dispensing, where the volume was locally adjusted to the pattern definition. After dispensing, the template was pressed into the still-liquid imprint material and held for 20 s under a pressure of 50 mbar to fill all the features. Thereafter, the imprint material was cured by UV-light irradiation through the transparent template, followed by demolding. Oxygen reactive ion etching to remove the imprinted resist was performed in an Elektrotech PF 340 apparatus (8 mTorr, 50 W, 20 sccm $O_2$).

*Surface-Initiated ATRP of PEGMA from Nanostructured Resist Films*: The ATRP initiator, 3-(chlorodimethylsilyl)propyl 2-bromo-2-methylpropionate (depicted in Scheme 1), was synthesized according to the literature.[53] For vapor phase deposition, 30 μL of ATRP initiator was put in a glass vial at the bottom of a desiccator containing the samples. The desiccator was subsequently evacuated during 10 min and left sealed under vacuum for 10 h. $CuBr_2$ was purchased from Aldrich and used as received. CuCl was purified by washing in glacial acetic acid and filtrated and rinsed with ethanol and diethyl ether. Poly(ethylene glycol) methacrylate with an average molecular weight of 360 Da was purchased from Sigma and subsequently purified from inhibitors by passing it through a basic alumina column. In a typical ATRP procedure 0.162 g of bipyridine was added to a mixture of 7.5 g of PEGMA 360 and 7.5 g of water. This solution was degassed by three freeze-thaw-pump cycles and later transferred, via a degassed syringe, to a second flask containing both CuCl (41.18 mg) and $CuBr_2$ (9.2 mg). The resulting mixture was stirred at ambient temperature for 30 min, until complete formation of a dark-brown complex. Subsequently, the reaction solution was transferred, via a degassed syringe, into an argon purged flask containing the ATRP-initiator functionalized samples. The polymerization was carried out for 1 h at room temperature under nitrogen.

*Functionalization of Brushes*: Before functionalization of the PEGMA brushes, the samples were immersed in dry toluene solution of 2-[methoxy(polyethyleneoxy)propyl]-trimethoxysilane (Aldrich) overnight under an Ar atmosphere in order to form PEG-bearing SAMs on the exposed $SiO_x$ regions. In order to confirm the successful formation of PEG SAMs this procedure was also carried out on a flat $SiO_x$ substrate, which was previously coated with an uniform resist film. This substrate was treated with the same lift-off procedure used for the patterned surfaces and later on it was immersed in PEG-bearing silane solution. The deposition of a uniform PEG SAM was confirmed by FTIR analysis (SI, Figure S3).

PEGMA brush films were reacted with succinic anhydride by an overnight reaction in 30 mg $mL^{-1}$ dry pyridine solution. Carboxylic acid derivatized PEGMA brush films were activated by immersion in an aqueous solution of EDC (1 M) and NHS (0.2 M) for 30 min. The samples were then rinsed with Milli-Q water, dried in a stream of nitrogen, and used immediately thereafter. For protein immobilization the samples were incubated in a phosphate buffer solution (PBS) solution of biotin-PEG (10) $NH_2$ (Sigma) overnight (1 μM). The biotin-functionalized surfaces were immersed in a PBS solution of streptavidin (1 μM, Sigma) or streptavidin-Cy2 presenting adsorption/excitation around 492 nm and fluorescence at 510 nm in the green region.

*Characterization*: Topography images of the fabricated PEGMA brush nanostructures were recorded by tapping-mode AFM using a Nanoscope Dimension (Veeco Digital Instruments, Santa Barbara CA, USA). A bearing analysis (Veeco Digital Instruments, Software 5.30, Santa Barbara CA, USA) was employed to evaluate the volume of PEGMA brush nanostructures after every functionalization step. This application generates a histogram based upon the occurrence of pixels at various heights on selected areas of the AFM images. By selecting all the pixels that extend above the plane represented by the surrounding surface the "bearing volume" of a feature can thus be calculated over the "bearing area" occupied by the same feature. An example of a typical bearing analysis on AFM images is reported in Figure S4, in the SI.

FTIR-spectra (spectral resolution of 8 $cm^{-1}$, 2048 scans) were obtained using a BIO-RAD FTS575C FTIR spectrometer equipped with a nitrogen-cooled cryogenic cadmium-mercury-telluride detector. Background spectra were obtained by scanning a clean silicon substrate. The dry thickness of uniformly grafted PEGMA brush films was measured using a computer-controlled null ellipsometer (Philips Plasmon) working with a He–Ne laser ($\lambda$ = 632.8 nm) at an incidence angle of 70°. The measurements were carried out at 22 °C and 30% relative humidity. The data were averaged over 100 points at the surface of each sample. SEM images were taken with a HR-LEO 1550 FEF SEM. No surface coating was applied. Fluorescent images of dye-labeled streptavidin/PEGMA brush structures were recorded with an Olympus IX71 fluorescence microscope.

## Supporting Information

Supporting Information is available from the Wiley Online Library or from the author.

## Acknowledgements

We gratefully acknowledge Dr. Szczepan Zapotoczny for fruitful discussions.

Received: December 6, 2010
Published online: April 14, 2011

[1] *Polymer Brushes: Synthesis, Characterization, Applications* (Eds: R. C. Advincula, W. J. Brittain, K. C. Caster, J. Ruhe), Wiley-VCH, Weinheim, Germany, **2004**.
[2] S. Edmondson, V. L. Osborne, W. T. S. Huck, *Chem. Soc. Rev.* **2004**, *33*, 14.
[3] B. Zhao, W. J. Brittain, *Prog. Polym. Sci.* **2000**, *25*, 677.
[4] Y. Tsujii, K. Ohno, S. Yamamoto, A. Goto, T. Fukuda, *Adv. Polym. Sci.* **2006**, *197*, 1.
[5] S. J. Ahn, M. Kaholek, W. K. Lee, B. LaMattina, T. H. LaBean, S. Zauscher, *Adv. Mater.* **2004**, *16*, 2141.
[6] M. Kaholek, W. K. Lee, S. J. Ahn, H. W. Ma, K. C. Caster, B. LaMattina, S. Zauscher, *Chem. Mater.* **2004**, *16*, 3688.
[7] M. Kaholek, W. K. Lee, B. LaMattina, K. C. Caster, S. Zauscher, *Nano Lett.* **2004**, *4*, 373.
[8] X. G. Liu, S. W. Guo, C. A. Mirkin, *Angew. Chem. Int. Ed.* **2003**, *42*, 4785.
[9] U. Schmelmer, A. Paul, A. Kuller, M. Steenackers, A. Ulman, M. Grunze, A. Gölzhäuser, R. Jordan, *Small* **2007**, *3*, 459.
[10] C. Thibault, V. Le Berre, S. Casimirius, E. Trévisiol, J. François, C. Vieu, *J. Nanobiotechnol.* **2005**, *3*, 7.
[11] H. D. Inerowicz, S. Howell, F. E. Regnier, R. Reifenberger, *Langmuir* **2002**, *18*, 5263.
[12] M. Mrksich, C. S. Chen, Y. N. Xia, L. E. Dike, D. E. Ingber, G. M. Whitesides, *Proc. Natl. Acad. Sci. USA* **1996**, *93*, 10775.
[13] A. Bernard, E. Delamarche, H. Schmid, B. Michel, H. R. Bosshard, H. Biebuyck, *Langmuir* **1998**, *14*, 2225.
[14] J. W. Lussi, C. Tang, P. A. Kuenzi, U. Staufer, G. Csucs, J. Vörös, G. Danuser, J. A. Hubbell, M. Textor, *Nanotechnology* **2005**, *16*, 1781.
[15] G. J. Zhang, T. Tanii, T. Zako, T. Hosaka, T. Miyake, Y. Kanari, T. W. Funatsu, I. Ohdomari, *Small* **2005**, *1*, 833.
[16] M. Arnold, E. A. Cavalcanti-Adam, R. Glass, J. Blummel, W. Eck, M. Kantlehner, H. Kessler, J. P. Spatz, *ChemPhysChem* **2004**, *5*, 383.
[17] T. M. Blättler, A. Binkert, M. Zimmermann, M. Textor, J. Vörös, E. Reimhult, *Nanotechnology* **2008**, *19*, 075301.
[18] Y. Cai, B. M. Ocko, *Langmuir* **2005**, *21*, 9274.
[19] Z. R. Taylor, K. Patel, T. G. Spain, J. C. Keay, J. D. Jernigen, E. S. Sanchez, B. P. Grady, M. B. Johnson, D. W. Schmidtke, *Langmuir* **2009**, *25*, 10932.
[20] A. Samadi, S. M. Husson, Y. Liu, I. Luzinov, S. M. Kilbey, *Macromol. Rapid Commun.* **2005**, *26*, 1829.
[21] S. F. Hou, Z. C. Li, Q. G. Li, Z. F. Liu, *Appl. Surf. Sci.* **2004**, *222*, 338.
[22] S. Zapotoczny, E. M. Benetti, G. J. Vancso, *J. Mater. Chem.* **2007**, *17*, 3293.
[23] E. M. Benetti, H. J. Chung, G. J. Vancso, *Macromol. Rapid Commun.* **2009**, *30*, 411.
[24] D. Wouters, U. S. Schubert, *Angew. Chem. Int. Ed.* **2004**, *43*, 2480.
[25] M. Steenackers, A. Kueller, N. Ballav, M. Zharnikov, M. Grunze, R. Jordan, *Small* **2007**, *3*, 1764.
[26] R. S. Kane, S. Takayama, E. Ostuni, D. E. Ingber, G. M. Whitesides, *Biomaterials* **1999**, *20*, 2363.
[27] T. Farhan, W. T. S. Huck, *Eur. Polym. J.* **2004**, *40*, 1599.
[28] S. Y. Chou, P. R. Krauss, P. J. Renstrom, *J. Vac. Sci. Technol. B* **1996**, *14*, 4129.
[29] S. Y. Chou, P. R. Krauss, P. J. Renstrom, *Science* **1996**, *272*, 85.
[30] D. Resnick, S. V. Sreenivasan, C. G. Willson, *Mater. Today* **2005**, *34*.
[31] T. C. Bailey, S. C. Johnson, S. V. Sreenivasan, J. G. Ekerdt, C. G. Willson, D. J. Resnick, *J. Photopolym. Sci. Technol.* **2002**, *15*, 481.
[32] S. C. Johnson, T. C. Bailey, M. D. Dickey, B. J. Smith, E. K. Kim, A. T. Jamieson, N. A. Stacey, J. G. Ekerdt, C. G. Willson, *P. SPIE—Int. Soc. Opt. Eng. (Pt. 1, Emerging Lithographic Technologies VII)* **2003**, *5037*, 197.
[33] S. V. Sreenivasan, I. McMackin, F. Xu, D. Wang, N. Stacey, *Micro Magazine* Jan/Feb **2005**.
[34] A. del Campo, E. Arzt, *Chem. Rev.* **2008**, *108*, 911.
[35] K. Studer, C. Decker, E. Beck, R. Schwalm, *Prog. Org. Coat.* **2003**, *48*, 92.
[36] T. E. Patten, K. Matyjaszewski, *Adv. Mater.* **1998**, *10*, 901.
[37] S. Tugulu, P. Silacci, N. Stergiopulos, H. A. Klok, *Biomaterials* **2007**, *28*, 2536.
[38] H. W. Ma, M. Wells, T. P. Beebe, A. Chilkoti, *Adv. Funct. Mater.* **2006**, *16*, 640.
[39] X. S. Wang, S. P. Armes, *Macromolecules* **2000**, *33*, 6640.
[40] K. L. Robinson, M. A. Khan, M. V. D. Banez, X. S. Wang, S. P. Armes, *Macromolecules* **2001**, *34*, 3155.
[41] W. X. Huang, J. B. Kim, M. L. Bruening, G. L. Baker, *Macromolecules* **2002**, *35*, 1175.
[42] W. K. Lee, M. Patra, P. Linse, S. Zauscher, *Small* **2007**, *3*, 63.
[43] M. Mathieu, A. Friebe, S. Franzka, M. Ulbricht, N. Hartmann, *Langmuir* **2009**, *25*, 12393.
[44] M. Patra, P. Linse, *Nano Lett.* **2006**, *6*, 133.
[45] H. W. Ma, J. Hyun, Z. P. Zhang, T. P. Beebe, A. Chilkoti, *Adv. Funct. Mater.* **2005**, *15*, 529.
[46] H. W. Ma, J. Hyun, P. Stiller, A. Chilkoti, *Adv. Mater.* **2004**, *16*, 338.
[47] F. J. Xu, H. Z. Li, J. Li, Y. H. E. Teo, C. X. Zhu, E. T. Kang, K. G. Neoh, *Biosens. Bioelectron.* **2008**, *24*, 773.
[48] X. Wang, X. Xiao, X. H. Wang, J. J. Zhou, L. Li, J. Xu, *Macromol. Rapid Commun.* **2007**, *28*, 828.
[49] M. Veiseh, M. H. Zareie, M. Q. Zhang, *Langmuir* **2002**, *18*, 6671.
[50] S. Lan, M. Veiseh, M. Q. Zhang, *Biosens. Bioelectron.* **2005**, *20*, 1697.
[51] A. Arakaki, S. Hideshima, T. Nakagawa, D. Niwa, T. Tanaka, T. Matsunaga, T. Osaka, *Biotechnol. Bioeng.* **2004**, *88*, 543.
[52] F. Costantini, E. M. Benetti, R. M. Tiggelaar, H. J. G. E. Gardeniers, D. N. Reinhoudt, J. Huskens, G. J. Vancso, W. Verboom, *Chem. Eur. J.* **2010**, *16*, 12406.
[53] B. Lego, W. G. Skene, S. Giasson, *Langmuir* **2008**, *24*, 379.